# MicroRNA perturbation of the MRN complex buffers DNA damage response from VEGF signaling

Cristina Espinosa-Diez [1], RaeAnna Wilson [1], Namita Chatterjee [1], Clayton Hudson [1], Rebecca Ruhl [1], Christina Hipfinger [1], Erin Helms [1], Omar F. Khan [2,] Daniel G. Anderson [2] and Sudarshan Anand [1].

[1]Department of Cell, Developmental and Cancer Biology, Department of Radiation Medicine, Oregon Health and Sciences University (OHSU), 3181 SW Sam Jackson Park Road, Portland, Oregon 97239 Portland, OR, US.

[2]Department of Chemical Engineering, Institute for Medical Engineering and Science, David H Koch Institute for Integrative Cancer Research, Massachusetts Institute of Technology, Cambridge, Massachusetts 02139, USA

**Corresponding Author:**

Sudarshan Anand, PhD

Tel 503 494-8043

Email: anands@ohsu.edu

**Abstract**

MicroRNAs contribute to biological robustness by buffering cellular processes from external perturbations. Here we report an unexpected link between DNA damage response and angiogenic signaling that is buffered by two distinct microRNAs. We demonstrate that genotoxic stress-induced miR-494 and miR-99b inhibit the DNA repair machinery by targeting the MRE11a-RAD50-NBN (MRN) complex. Functionally, miR-494 and miR-99b affect telomerase activity, activate p21 and Rb pathways and diminish angiogenic sprouting *in vitro* and *in vivo*. Genetic and pharmacological disruption of VEGFR-2 signaling and the MRN complex reveal a surprising co-dependency of these pathways in regulating endothelial senescence and proliferation. miR-99b diminishes VEGF signaling, transcriptional responses and proliferation. Disruption of the MRN complex induces CD44, a known driver of senescence and regulator of VEGF signaling. Our work identifies a putative miR-facilitated mechanism by which endothelial cells can be insulated against VEGF signaling to facilitate the onset of senescence.

## Introduction

Accumulation of DNA damage can overwhelm the repair machinery and lead to senescence (Bautista-Nino, Portilla-Fernandez et al. 2016). Endothelial senescence leads to progressive damage and deterioration of cellular structure and function over time (Regina, Panatta et al. 2016) (Gates, Strain et al. 2009). Two major pathways of senescence in endothelial cells are replicative senescence and stress induced senescence. Replicative senescence is one of the hallmarks of aging and is associated to telomere shortening. Stress-induced premature senescence (SIPS) is triggered by external stimuli, including oxidizing agents and radiation, both of which can induce DNA damage and cell cycle arrest.

Recent studies indicate that DNA repair proteins in ECs, such as ATM kinase and histone H2AX, have an inherently pro-angiogenic role (Economopoulou, Langer et al. 2009, Okuno, Nakamura-Ishizu et al. 2012). For example, ATM deficiency kinase decreases tumor angiogenesis while enhancing the anti-angiogenic action of VEGF blockade, suggesting that pathological neoangiogenesis requires ATM. Similarly, global or EC specific deletion of the histone H2AX in mice results in a substantial decrease of pathological angiogenesis in proliferative retinopathy, hindlimb ischemia and tumor angiogenesis. These findings suggest that key regulators of DNA damage repair (DDR) modulate pathological angiogenesis. Recently, we identified a seven-miR signature of DNA damage in ECs induced in common by genotoxic stress, oxidative stress and radiation (Wilson, Espinosa-Diez et al. 2016). We demonstrate that two DNA damage induced miRs from this signature, miR-494 and miR-99b, regulate endothelial cell cycle, senescence, survival and sprouting angiogenesis *in vitro* and *in vivo*. Using gene expression arrays, we identified the MRE11a-RAD50-NBN (MRN) complex, a critical DNA

damage response checkpoint (Uziel, Lerenthal et al. 2003, Williams and Tainer 2007), as a primary target of these miRs.

MRN acts as a sensor of DNA double strand breaks (DSB), initiating Homologous Recombination (HR) or Non-Homologous-End-Joining (NHEJ) pathway. Once MRN detects DSBs, it tethers the ends, activates and recruits DNA damage response proteins such as ATM (Williams, Williams et al. 2007) (Lafrance-Vanasse, Williams et al. 2015). Interestingly, MRN is also associated with telomere maintenance, playing a role in the formation and disassociation of the t-loops (Dimitrova and de Lange 2009, Porro, Feuerhahn et al. 2014). The MRN complex relationship with aging and cell senescence has been described (Ju, Lee et al. 2006, Gao, Singh et al. 2015), however its role in endothelial cell and vascular pathology is unclear. Similarly, while several miRs have been shown to be involved in EC senescence (Boon and Dimmeler 2015, Regina, Panatta et al. 2016, Santulli 2016), proliferation, viability and migration (Fish and Srivastava 2009) (Shi, Li et al. 2010) (Landskroner-Eiger, Moneke et al. 2013), our work identifies a specific link between DDR driven induction of miR-494, miR-99b, the MRN complex, EC senescence and angiogenic signaling.

Our results indicate that DNA damage induces a miR mediated regulatory process that can inhibit repair, diminish telomerase activity and therefore, enhance cellular senescence. These phenomena are also exacerbated by the ability of these miRs to interfere with VEGF signaling and transcription, thereby amplifying the anti-angiogenic effect of these miRs. We propose that miR-494 and miR-99b serve to insulate replicative senescence from growth factor driven proliferation by virtue of their effect on the MRN complex and DDR.

## Results

### DNA damage induced miRs drive EC senescence and inhibit angiogenesis

We previously reported a seven microRNA signature (miR-103, miR-494, miR-99b, miR-21, miR-224, miR-92a and let-7a) specifically upregulated in ECs after radiation, hydrogen peroxide and cisplatin treatment. Among these, we found that miR-99b and miR-494 are both transcribed rapidly in human umbilical vein endothelial cells (HUVECs) in response to $\gamma$-radiation with maximal induction occurring at a lower (2 Gy) dose of radiation. (Figure 1A-B).

To understand the role of these two miRs, we transfected HUVECs with the corresponding miR mimics and observed a significant increase in senescence associated β-galactosidase (Figure 1C). This phenotype was also observed in human microvascular endothelial cells (HMVECs) (Supplementary Figure 1). Phalloidin staining in HUVECs after 48 hours of miR-494 treatment revealed flattened and multinucleated cells (Figure 1D), a morphological phenotype associated with stress dependent senescence. Consistent with these findings, we observed an increase in the cell cycle regulator p21 as well as a decrease in Rb hyperphosphorylation (Figure 1E). Importantly, we also observed a decrease in telomerase activity (Figure 1F), confirming that the expression of miRs-494 and 99b induced senescence in ECs.

Next we investigated whether this senescence induction in ECs had functional consequences on angiogenesis. Transfection of either miR-99b or miR-494 mimic inhibited sprouting angiogenesis in a 3D-fibrin bead assay (Figure 1G). To determine if this inhibition of angiogenesis occurred *in vivo*, we implanted bFGF containing Matrigel plugs in mice and treated the mice with miR-494 mimic in EC targeted 7C1 nanoparticles

(Dahlman, Kauffman et al. 2014, Wilson, Espinosa-Diez et al. 2016). We found more than a 50% decrease in CD31 staining in miR-494 treated plugs compared to the control miR mimic treated group (Figure 1H). These experiments suggest that miRs -494 and -99b not only induce EC senescence but also cause a reduction in angiogenesis.

**miR-494 and miR-99b target the MRN DNA repair complex**

To analyze the possible targets of these miRs responsible for this phenotype, we ectopically expressed these two miRs in HUVECs and analyzed gene expression using a DNA damage array (Supplementary Figure 2). Interestingly, we identified three common targets: MRE11a, RAD50 and NBN. RNA hybrid modeling suggested putative binding sites for both miRs on all three target 3'UTR regions (Supplementary Figures 3-4). Both miR-494 and -99b directly bound MRE11A mRNA, and to a lesser extent, RAD50 and NBN mRNAs, as measured by a miRTrap assay (Clontech) (Figure 2A). Consistent with this finding, transfection of miR mimics decreased MRN RNA levels by qRT-PCR (Figure 2B) and protein levels as measured by a western blot (Figure 2C). We corroborated the interaction of these miRs with their targets by cloning the 3´-UTRs in luciferase reporter vectors, and co-transfecting them in HEK-293T cells. Either of the miRs transfected alone was able to decrease the luciferase activity downstream of the MRN 3´-UTR reporter (Figure 2D). Finally, miR-494 transfected HUVECs showed a decrease in MRE11a nuclear foci (Figure 2E).

miRs typically regulate several target mRNA transcripts making their functional attribution challenging (Bartel 2009), (Li, Cassidy et al. 2009, Inui, Martello et al. 2010, Osella, Bosia et al. 2011, Ebert and Sharp 2012). To address this, we used a target protector, a locked nucleic acid (LNA) stabilized oligonucleotide, that binds completely to a specific miR-binding site on a single target mRNA, to rescue it from the negative regulation of the miR.

We confirmed that in the presence of the MRE11A target protector, miR-494 did not decrease MRE11A RNA levels (Supplementary Figure 5A). Functionally, the MRE11A target protector significantly restored the telomerase activity and to a lesser extent the senescence associated $\beta$-gal levels in miR-494 transfected cells (Supplementary Figure 5B-C).

**Disruption of the MRN complex phenocopies miR-494 and miR-99b effects**

We then sought to determine if disruption of the MRN complex using siRNAs (Supplementary Fig 6A-B) or small molecule inhibitors resulted in a similar phenotype. Indeed, silencing each of the components of the MRN complex induced senescence and impaired telomerase activity (Figure 3A-B). Similar to our miR effects, siRNAs targeting MRE11a and NBN inhibited sprouting angiogenesis significantly (Figure 3C). Furthermore, Mirin-1, a small molecule inhibitor specific to MRE11a (Garner, Pletnev et al. 2009), induced senescence in HUVECs (Figure 3D). Consistent with the effects in HUVECs, siRNAs targeting the MRN complex and Mirin-1 all induced senescence in HMVECs, (Supplementary Fig 7A-B). Taken together our data indicate that miR -494 and -99b induce senescence, impair telomerase activity and affect angiogenesis, likely by their effects on the MRN pathway.

To understand the shared molecular pathways that may drive senescence downstream of miR-494, miR-99b and the MRN complex, we utilized a human senescence gene signature array. We found 6 genes with similar changes across both the miR and siRNA treatment groups (Supplementary Fig 8A). Interestingly, CD44, a known negative regulator of VEGF signaling (Ponta, Sherman et al. 2003, Tremmel, Matzke et al. 2009), was the most significantly upregulated gene in the four groups. This increase in gene expression

was also reflected by increased cell surface expression of CD44 (Supplementary Figure 8B).

**MRN-VEGF codependency**

While disruption of DNA damage response (DDR) in ECs can modulate both pathological and developmental angiogenesis via VEGF (Economopoulou, Langer et al. 2009, Okuno, Nakamura-Ishizu et al. 2012), it is not clear if this phenomenon is unique to histone H2AX and/or ATM or if targeting MRN would also influence VEGF signaling. To address this, we silenced VEGF-receptor 2 (VEGFR2) and tested the ability of miR-99b, miR-494 or the specific siRNAs against the MRN complex to induce senescence. Surprisingly, knockdown of VEGFR2 diminished the senescence promoting activities of miR-494, miR-99b, siRNAs targeting the MRN and Mirin-1 (Fig 4A-C). Similarly, combinatorial disruption of both VEGFR2 and MRE11a either with siRNA (Fig 4D) or with Mirin-1 and Vandetanib, a small molecule inhibitor for VEGFR2 (Fig 4E), led to a decrease in proliferation of HUVECs. We suspected that the disruption of the MRN complex destabilized the activity of VEGFR2, either at the signaling level or at the transcriptional level. Interestingly, we found that miR-99b expression blocked specifically VEGF early gene transcription (Fig 4F). miR-99b also decreased VEGF-dependent phosphorylation of ERK (Figure 4G). This dampening effect of VEGF induced ERK activation was also recapitulated by Mirin-1 (Fig 4H).

These results demonstrate that the DNA repair pathway and the MRN complex have an essential functional role in angiogenesis and we propose that we can exploit this DNA repair-VEGF pathway codependency for future antiangiogenic therapies. Genotoxic stress agents induce DNA damage in ECs; however, they also increase expression of miR-99b and miR-494. These two miRs lead to senescence by targeting the DNA repair complex MRN. Moreover, disruption of MRN decreases proliferation and transcription of early

VEGF genes likely by targeting ERK phosphorylation (Fig 5) and amplifying the induction of senescence and inhibition of angiogenesis.

## Discussion

We have postulated that a network of stress-dependent miRs target DNA repair pathways leading to impaired angiogenesis (Wilson, Espinosa-Diez et al. 2016). Among this group of stress-induced miRs, miR-99b and miR-494 lead to senescence, likely through MRN disruption. miR-494 has been shown to be highly upregulated in retinoblastoma (Zhao, Yang et al. 2009), cardiovascular pathologies such as cardiac injury (Wang, Zhang et al. 2010) and in atherosclerotic lesion development (Wezel, Welten et al. 2015). miR-494 has also been reported as an angiogenesis inhibitor, supporting our data here (Asuthkar, Velpula et al. 2014, Welten, Bastiaansen et al. 2014, Chen, Zhao et al. 2015). Recently, Esser et al demonstrated that miR-494 is downregulated in ECs treated with the pro-angiogenic factor BMP4, in opposition to an increase in the pro-angiogenic miR-126 (Esser, Saretzki et al. 2017). miR-494 has been implicated in tumor senescence and the development of resistance to radiation and chemotherapy (Comegna, Succoio et al. 2014) (Weng, Yu et al. 2016) (Ohdaira, Sekiguchi et al. 2012) (Liu, Li et al. 2015).

In EC-progenitors, miR-99b affects the expression of PECAM-1 and VE-cadherin (Kane, Howard et al. 2012). miR-99b also modulates β-catenin in endothelial junctions (Zhuang, Peng et al. 2016). Interestingly, miR-99b expression has been proposed as a prognostic marker to assess the response to VEGFR2 Tyrosine Kinase Inhibitors (TKI). Lukamowicz-Rajska et al described higher expression of miR-99b-5p in clear cell renal cell carcinoma (CCRC) patients with complete response to TKI treatments (Lukamowicz-Rajska, Mittmann et al. 2016) compared to partial or non-responders. Another example is dermal wound healing, where TK pathways have decreased signaling. Prior studies proposed that miR-99b targets several members of the IGFR1/AKT/mTOR signaling pathway. They demonstrated that miR-99b was downregulated in the early phases of wound healing likely facilitating cell proliferation (Jin, Tymen et al. 2013). We propose here that miR-99b

expression is leading to senescence through MRN disruption, but that its effect on the VEGFR2/ERK signaling pathway enhances the anti-angiogenic phenotype. Similarly, our observations of miR-99b diminishing a specific VEGF-dependent early-gene signature (Schweighofer, Testori et al. 2009), also suggests that the induction of miR-99b in complete responders can enhance the effect of VEGFR2 TKIs.

We find that miR-494 and miR-99b target MRE11a, NBN and RAD50 to affect EC senescence and sprouting angiogenesis. EC senescence leads to dysfunction in cardiovascular diseases (Minamino, Miyauchi et al. 2002, Kurz, Decary et al. 2004). Loss of function mutations in the MRN genes cause inherited genetic disorders that are characterized by elevated sensitivity of patients' cells to radiation damage (O'Malley, Li et al. 2003, Dzikiewicz-Krawczyk 2008). Interestingly, there is some evidence that NBN disruption has an anti-angiogenic effect *in vivo* (Araki, Yamashita et al. 2010). Our observations also imply that the senescence phenotype maybe mediated by the increase in CD44 expression on the cell surface (Mun and Boo 2010). CD44 is a known regulator of endothelial interactions with leukocytes in addition to its other critical roles in EC junction integrity (Flynn, Michaud et al. 2013). Induction of CD44 in response to DNA damage by miR disruption of the MRN complex may increase adhesiveness of the endothelium (Orian-Rousseau, Chen et al. 2002, DeLisser 2009).

Although the role of MRN in DNA damage repair and likely effects on senescence are well studied, emerging studies have implicated deficient telomere maintenance as leading to senescence when MRN function is compromised. For example, decreased MRE11a has been shown to increase T-cell aging in arthritis due to compromised telomere maintenance and heterochromatin unraveling (Li, Shen et al. 2016). Recent structural studies also shed light on how the phosphorylation of NBS influences its interaction with TRF2 and dictates

the repair of telomeres (Rai, Hu et al. 2017). RAD50 downregulates the association of TRF1 from telomeres and also contribute to maintain telomere length (Wu, Xiao et al. 2007). We saw a decrease in telomerase activity across miRs and siRNAs experiments targeting the MRN complex. Moreover, the MRE11a target protector largely restored this function, implying this was the miR-494 target responsible for the compromised telomerase activity. Therefore, we suspect that the telomere maintenance function of the MRN complex drives the EC senescence downstream of miRs-494 and miR-99b induced by DNA damage.

Our observations indicate that the function of these miRs in regulating telomerase activity and EC senescence may depend on the expression of VEGFR2. This is surprising, since expression of VEGFR2 may steer cells into a robust replication program rather than a cell cycle exit characteristic of senescence. However, it is possible that replication stress and DNA damage are enhanced in the presence of these miRs. Similarly, our findings demonstrate a decrease in MRN activity either by miR-99b induction or Mirin-1 affects the VEGFR signaling at the level of P-ERK and a subset of the VEGF early response genes. These data argue that the MRN pathway and the VEGFR2 signaling cross-talk functions as a threshold to determine the level of DNA damage in ECs. In the presence of significant DNA damage the MRN pathway is disrupted and the VEGF signaling is diminished thereby decreasing angiogenesis.

It is possible that during physiological aging, increase in miR-494 and miR-99b levels render the ECs less responsive to VEGF levels and therefore, decrease angiogenic responses. We envision that this senescence associated decrease in VEGF sensitivity functions in a feedforward loop and contributes to cardiovascular aging.

## Material and Methods

### Cell Culture and Reagents

HUVECs (Lonza) were cultured in EGM-2 media (Lonza) supplemented with 10% Fetal Calf Serum (Hyclone). ASMCs (Lonza) were cultured in Medium 231, supplemented with Smooth muscle growth serum (GIBCO). Cells were tested and found negative for mycoplasma contamination before use in the assays described. Mirin-1 and Vandetanib were purchased from Cayman Chemical and Selleckchem respectively. VEGF was purchased from PeproTech, Inc.

### miRs/anti-miRs/siRNAs.

miR mimics, inhibitors and respective controls were purchased from Life Technologies and Exiqon. For *in vivo* studies, high-performance liquid chromatography-purified miRs were purchased from Life Technologies in bulk quantities. siRNAs against MRE11a, RAD50 and NBN were purchased from Life Technologies. VEGFR2 Gapmer and MRE11a target protector were purchased from Exiqon.

### Vectors/Plasmids.

MRE11a Luciferase-3-UTR plasmid was purchased from SwitchGear Genomics. RAD50 and NBN luciferase constructs were generated by cloning the entire 3'UTR regions into pmiR-REPORT vector (Ambion). Luciferase assay reagents were purchased from SwitchGear Genomics and Promega.

### Transfection

Cell were transfected at 50–60% confluence using standard forward transfection protocols using RNAimax reagent (Life Technologies) for miRs, siRNAs or gapmers and Lipofectamine 2000 for plasmid or plasmid RNA dual transfections. Typically 50 nM RNA

and 1–2 µg plasmid DNA were used for transfections. Target protectors were transfected at a concentration of 50 nM or equivalent to the miR amounts.

**Radiation of cells**

Cells were irradiated on a Shepherd$^{137}$cesium irradiator at a rate of B166 1.34 cGy min.

**β-Gal Senescence assay**

HUVEC were transfected for 48 hours with the correspondent microRNA or siRNA. After this time cells were washed with cold PBS and then stained for β-galactosidase activity following manufacturer's protocol (Senescence Cells Histochemical Staining Kit, Sigma).

**Telomerase activity assay**

Cells were transfected with microRNAs or siRNAs for 24 hours. Cells were lysed and processed according to manufacturer´s instructions (Quantitative Telomerase Detection Kit, Allied Biotech). The telomerase activity level in the cell extract was determined through its ability to synthesize telomeric repeats onto an oligonucleotide substrate. The resultant extended product was subsequently amplified by polymerase chain reaction (PCR).

**Western blot and densitometric analysis**

After treatment, cells were washed in phosphate-buffered saline (PBS) and lysed in RIPA buffer (Sigma) supplemented with Complete Protease inhibitor cocktail (ROCHE) and Phosphatase inhibitors cocktail 2 and 3 (Sigma). Lysed cells were harvested by scraping, and proteins were analyzed by Western blot. Equivalent amounts of protein were loaded on a 4–12% gradient SDS-polyacrylamide gel (BioRAD) and transferred for 30 min in a TransBlot turbo (BioRAD) onto Nitrocellulose membranes. Membranes were blocked in 5% milk or 3% BSA and incubated with antibodies as indicated: MRE11a (Cell Signaling, 4847, 1:1000), RAD50 (Cell Signaling, 3427, 1:1000), NBS1 (Cell Signaling, 14956,

1:500), p-ATM (Cell Signaling, 4526, 1:500), H2AX (Abcam, 11174, 1:500), p21 (Cell Signaling, 2947, 1:1000), P-Rb (Cell Signaling, 9301, 1:500), ERK1/2 (Cell Signaling, 9102, 1:1000), P-ERK1/2 (9101, 1:1000). β-actin (Sigma, A5316, 1:10,000 1□h RT) was used as a housekeeping control for the total levels of protein loaded. Membranes were washed in TBST and incubated with secondary antibodies from Licor Biosciences. Licor antibodies used were goat anti mouse 925-68020 (1:15,000) and goat anti rabbit 925-32211 (1:15,000). Blots were scanned on the Licor Odyssey scanner according to manufacturer's instructions.

**RNA extraction, RT-PCR, miR Profiling**

Total RNA and microRNA were isolated using a miRVana microRNA isolation kit (Ambion). Reverse transcription was performed using TaqMan™ Advanced cDNA Synthesis Kit (Life Tech) according to the manufacturer's instructions. RT-PCR was performed using multiplexed TaqMan primers (Applied Biosystems). The relative quantification of gene expression was determined using the $2^{-\Delta\Delta Ct}$ method (35). Using this method, we obtained the fold changes in gene expression normalized to an internal control gene, GAPDH or U6 snRNA, respectively. For target analysis a 92 gene DNA damage array (Life tech, 4418773) was used and for senescence phenotype profiling the Human Cellular Senescence array was utilized (SA Biosciences).

**miR-TRAP/RISC TRAP assay.**

293 T cells were co-transfected with a plasmid coding for a flag-tagged dominant negative GW418 mutant (Clontech kit #632016) along with a control mimic, miR-99b or miR-494 mimic according to kit instructions. Twenty-four hours later the RNA protein complexes were crosslinked and the RISC complex was immunoprecipitated using an anti-FLAG antibody and RNA was isolated for quantitative real-time PCR of target genes. The fold

enrichment was calculated using pre and post IP controls as well as normalization to the control mimic pull-downs.

**3-D Angiogenic Sprouting Assay**

Early passage HUVECs were coated on cytodex-3 beads (GE Healthcare) at a density of 10 million cells/40 μl beads and incubated in suspension for 3-4 hours with gentle mixing every hour. They were plated on TC treated 6 well dishes overnight and resuspended in a 2mg/ml fibrin gel with 200,000 human smooth muscle cells. The gel was allowed to polymerize and complete EGM-2 media was added. Sprouts were visualized from days 3-4 via confocal imaging after overnight incubation with FITC labeled *Ulex europaeus* lectin (Vector labs). Immunofluorescence imaging was performed on a Yokogawa CSU-W1 spinning disk confocal microscope with 20 0.45 Plan Fluor objective (Nikon).

**Flow cytometry**

CD44 expression was analyzed by flow cytometry in HUVECs transfected with miR-494 for 48 hours. Cells were washed in PBS and trypsinazed. Cells were incubated in blocking solution (0.5 %BSA/ 10% goat serum) for 30 min and then incubated for 1 hour in primary antibody-PEcy7 conjugated (CD44, BD, 560533) prepared in blocking solution. Then cells were washed 3X with PBS. Cells were analyzed in a CANTOII equipment.

**Immunofluorescence and microscopy**

In some experiments, CD31a and MRE11a were visualized using immunofluorescence staining from OCT sections. Slides were fixed with 4% PFA and stained overnight for CD31 488 (BD bioscience 611986 1:200 o/n), MRE11a (Cell Signaling Technology 1:100) and Phalloidin Alexa 647 (1:50). For MRE11a antibody, following day fixed cells were incubated with Goat anti-Rabbit Alexa 488 (1:500) in 5%BSA/TBS for 1 hour. Imaging was performed on a Nikon Spectral C1 confocal microscope (Nikon C1si with EZC1 acquisition

software, Nikon Instruments) with Plan Apo 10X/0.45 air, Plan Apo 20X/0.75 air, and Plan Apo 60X/1.40 oil objective lenses (Nikon). Some immunofluorescence imaging was performed on a Yokogawa CSU-W1 spinning disk confocal microscope with 20 0.45 Plan Fluor objective (Nikon). All images were taken with a channel series. Images were analyzed with Image J software for quantitation.

**P-ERK Elisa**

We measured the abundance of p-ERK with an ELISA kit (PathScan® Phospho-p44/42 MAPK (Thr202/Tyr204) Sandwich ELISA, Cell Signaling Technology) following manufacturer's instructions.

***In vivo* assays**

All animal work was approved by the OHSU Institutional Animal Use and Care Committee. Immune-compromised 8-10 week old female nu/nu mice were purchased from Jackson Labs. Growth factor reduced Matrigel (BD) with 400 ng/ml recombinant human bFGF (Millipore) was injected subcutaneously in nu/nu mice. Mice were injected i.v. with 7C1-nanoparticles containing miR-494 or control miR (~1mg/kg, i.v) 3 or 4 days after plugs were implanted. At day 7 mouse tissues were harvested and processed to obtained RNA or frozen in OCT for tissue staining.

**Statistics**.

All statistical analysis was performed using Excel (Microsoft) or Prism (GraphPad). Two-tailed Student's t-test was used to calculate statistical significance. Variance was similar between treatment groups.

## Figure Legends

### Figure 1: DNA damage induced miRs-494, 99b drive EC senescence and inhibit angiogenesis

**A**. pri-miR expression in HUVECs after 1h and 3h post 2 Gy radiation. Graph depicts pri-miR-99b and pri-miR-494 in HUVEC analyzed by qPCR. **B**. pri-miR expression radiation-dose response. Graph shows pri-miR-99b and pri-miR-494 at 1h post-radiation. **C**. $\beta$-Gal assay in HUVEC transfected for 48h with miR-99b and miR-494. Graph shows % mean + SEM of $\beta$-gal positive cells for at least hundred cells analyzed **D**. Phalloidin staining. HUVECs were transfected with miR-NC and miR-494. After 48h, cells were fixed and stained with anti-phalloidin antibody (red) and DAPI (blue) as indicated. Bars depict % mean cellular area + SEM. **E**. Representative western-blot of p21 and pRB in HUVEC. **F.** Telomerase activity assay. HUVEC were transfected with miR-99b and miR-494 for 48h. Bars depict % mean + SEM of Telomerase activity. **G**. Fibrin bead 3D assay. Transient transfected HUVEC were cultured with fibrin-beads in the presence of Smooth Muscle Cells over 5 days. The images show representative beads for each condition. Bars depict mean +SEM of lectin area analyzed across at least 25 beads per group. **H**. CD31 staining *in vivo*. Matrigel plugs were implanted in nude mice and treated with miR-NC or miR-494 7C1 nanoparticles after 4 days, for 2 consecutive days. Mice were sacrificed at day 7 and plugs were harvested for tissue sections. Angiogenesis was measured by staining matrigel plugs sections with anti-CD31 (green) and $\alpha$SMA (red) and DAPI (blue). Quantification of CD31 area from at least three mice per group are shown. Bars show mean + SEM. *$p \leq 0.05$.

**Figure 2. miR-99b and miR-494 target the MRN complex in ECs**

**A.** miR-TRAP immunoprecipitation. Bars depict mean of mRNA levels + SEM analyzed by qRT-PCR in HEK-293T cells transfected with miR-99b and miR-494 for 24h. **B.** Target validation in HUVEC. Graphs depict mean mRNA levels + SEM of the three MRN complex members. **C.** Representative western-blot of MRE11a and RAD50 after 48h transfection. **D.** Luminescence from 3'-UTR-luciferase constructs for MRE11a, RAD50 and NBS 24h after transfection with miR-99b or miR-494. Graph represents mean +SEM of 3 independent experiments, *p≤ 0.05. **E.** MRE11a immunostaining. HUVECs were plated on glass coverslips and 24h later transfected with miR-494 or miR negative control. After 48h cells were fixed and stained with MRE11a antibody. Scale bar represents 10 µm. Bar graph depicts average foci/ cell + SEM.

**Figure 3. Disruption of the MRN complex phenocopies miR-494 and 99b effects**

**A.** $\beta$-Gal assay in HUVEC transfected for 48 hours with different siRNAs against MRE11a, RAD50 and NBN and the respective siRNA control. Graph shows % mean + SEM of $\beta$-gal positive cells for at least hundred cells analyzed. **B.** Telomerase activity assay in HUVEC transfected for 48h with specific siRNAs against MRE11a, RAD50 and NBN and the respective siRNA control. Bars depict % mean + SEM of Telomerase activity. **C.** Fibrin bead 3D assay. The images show representative beads for each condition. Bars depict mean +SEM of lectin area analyzed across at least 25 beads per group. **D.** $\beta$-Gal assay in HUVEC treated with Mirin-1 for 48 hours. Graph shows % mean + SEM of $\beta$-gal positive cells for at least hundred cells analyzed. *p≤ 0.05.

**Figure 4. The MRN and VEGF signaling pathways are dependent on each other**

**A.** β-Gal assay in HUVEC co-transfected for 48h with miR-99b or miR-494 and VEGFR2 receptor gapmer. **B.** $\beta$ -Gal assay in HUVEC co-transfected for 48h with siRNAs against MRE11a or NBN and VEGFR2 receptor gapmer. Graph shows % mean + SEM of $\beta$ -gal positive cells for at least hundred cells analyzed. *p≤ 0.05 **C.** $\beta$ -Gal assay in HUVEC transfected for 48h with VEGFR2 gapmer and treated with Mirin-1 (50 $\mu$ M) for 24h. Graphs show % mean ± SEM of $\beta$ -gal positive cells for more than 100 hundred cells analyzed. *p≤ 0.05. **D.** Cell proliferation assay in HUVECs transfected for 48h with VEGFR2 gapmer and treated with Mirin-1 (50 $\mu$ M) for 24h **E.** Cell proliferation assay in HUVECs treated with VEGFR2 inhibitor Vandetanib (10 $\mu$ M) alone or in combination with Mirin-1 (50 μM). **F.** mRNA levels of VEGF-early response genes after miR-99b expression. HUVECs were transfected for a total of 48h. At 24h cells were starved overnight and then treated with VEGF (50ng/ml) for 3h. Graphs depict mean mRNA levels + SEM. *p≤ 0.05. **G.** Representative P-ERK Elisa assay. HUVECs were transfected for a total of 48h. At 24h cells were starved overnight and then treated 10 min with VEGF (50ng/ml). P-ERK levels were assayed using an ELISA quantified via colorimetric detection at 450 nm. Graphs depict mean p-ERK levels + SEM. *p≤ 0.05. H. HUVECs were starved overnight before VEGF treatment and treated with Mirin-1. Then cells were treated 10 min with VEGF (50ng/ml) and p-ERK levels were measured as in G. Graphs depict mean p-ERK levels + SEM. *p≤ 0.05.

**Figure 5. Schematic summary – DNA damage repair and VEGF signaling cross talk**

Genotoxic stress in ECs induces DNA damage that leads to increase expression of miR-99b and miR-494. These microRNAs target the MRN complex inducing EC senescence. In ECs when VEGF/VEGFR2 signaling pathway is activated ERK1/2 is phosphorylated, leading to increased proliferation. However when MRN complex is decreased by miRs or

siRNAs or Mirin-1, ERK pathway is also decreased. On the contrary, when VEGF signaling is inhibited increased DNA damaged does not lead to senescence. Therefore we hypothesize that MRN and VEGF are codependent and that crosstalk between the two pathways dictate endothelial senescence.

**Supplementary Figure 1. Senescence phenotype in HMVEC cells: A.** $\beta$-Gal assay in HMVEC transfected for 48 hours with **A.** miR-C, miR-99b or miR-494. Graphs show % mean $\pm$ SEM of $\beta$-gal positive cells for at least hundred cells analyzed.

**Supplementary Figure 2. microRNA targets validation: A.** Heat map represents mRNAs up or down-regulated by miR-99b and miR-494 analyzed by TaqMan q-PCR based Human DNA Repair Array.

**Supplementary Figure 3: RNA hybrid models for miR-494**

**A.** mRNA sequence of human MRE11a, **B.** RAD50 and **C.** NBN. Binding sites are highlighted in red. MRE11a-miR-494 target blocker was designed against the site highlighted in red and underlined.

**Supplementary Figure 4: RNA hybrid models for miR-99b**

**A.** mRNA sequence of human MRE11a **B.** RAD50 and **C.** NBN. Binding sites are highlighted in red.

**Supplementary Figure 5. MRE11a target protector validation**

**A.** HUVECs were transfected with a target protector for miR-494 binding site in MRE11a-3´-UTR or a scrambled control, and the corresponding miRs during 24 hours. Bar graph depicts mean +SEM of the three members of MRN complex. **B**. Telomerase activity assay. HUVEC were transfected with a target protector for miR-494 binding site in MRE11a-3´-UTR or a scrambled control, and the corresponding miRs for 48 hours. Bars depict %

mean + SEM of Telomerase activity. **C.** $\beta$ -Gal assay in HUVEC transfected with a target protector for miR-494 binding site in MRE11a-3'-UTR or a scramble control, and the corresponding miRs for 48 hours. Graph shows % mean + SEM of $\beta$ -gal positive cells for at least hundred cells analyzed.

**Supplementary Figure 6. siRNA validation**

**A.** HUVEC were transfected with specific siRNAs against MRE11a, RAD50 and NBN and the respective siRNA control during 24 hours. Bar graph depicts mean +SEM of the three members of MRN complex. **B**. Representative western blot of MRE11a, RAD50 and P-Rb in HUVEC transfected for 48 hours with specific siRNAs against MRE11a, RAD50 and NBN and the respective siRNA control.

**Supplementary Figure 7. Senescence phenotype in HMVEC cells**

β-Gal assay in HMVEC transfected for 48 hours with **A**. siRNA-NC, siRNA-MRE11a or siRNA-NBN or **B**. treated with Mirin-1 (50 μM) for 24h. Graphs show % mean ± SEM of β-gal positive cells for at least hundred cells analyzed.

**Supplementary Figure 8. Senescence gene profiling**

**A.** Heat map represents the 6 mRNAs commonly altered by miR-99b, miR-494, siRNA-MRE11a and siRNA-RAD50 analyzed on TaqMan q-PCR based Human Senescence gene Array. **B.** Representative CD44 histogram analyzed by Flow cytometry. HUVECs were transfected for 48 hours with miR-494 and its respective control.

**Acknowledgements**

We thank Sergio Fazio and Stephen Lloyd (OHSU) for useful discussions. We thank Shushan Rana and Katherine Kelly (OHSU) for comments on the manuscript. We thank the OHSU Advanced Light Microscopy Core, Knight Cancer Institute Flow Cytometry Core and the Gene Profiling Shared Resource for technical help and useful discussions. S.A. is supported by US NIH grant R00HL112962, an innovative research grant from the American Heart Association (17IRG33400218)

## Bibliography

Araki, K., T. Yamashita, N. Reddy, H. Wang, W. M. Abuzeid, K. Khan, B. W. O'Malley, Jr. and D. Li (2010). "Molecular disruption of NBS1 with targeted gene delivery enhances chemosensitisation in head and neck cancer." Br J Cancer **103**(12): 1822-1830.

Asuthkar, S., K. K. Velpula, A. K. Nalla, V. R. Gogineni, C. S. Gondi and J. S. Rao (2014). "Irradiation-induced angiogenesis is associated with an MMP-9-miR-494-syndecan-1 regulatory loop in medulloblastoma cells." Oncogene **33**(15): 1922-1933.

Bartel, D. P. (2009). "MicroRNAs: target recognition and regulatory functions." Cell **136**(2): 215-233.

Bautista-Nino, P. K., E. Portilla-Fernandez, D. E. Vaughan, A. H. Danser and A. J. Roks (2016). "DNA Damage: A Main Determinant of Vascular Aging." Int J Mol Sci **17**(5).

Boon, R. A. and S. Dimmeler (2015). "MicroRNAs in myocardial infarction." Nat Rev Cardiol **12**(3): 135-142.

Chen, S., G. Zhao, H. Miao, R. Tang, Y. Song, Y. Hu, Z. Wang and Y. Hou (2015). "MicroRNA-494 inhibits the growth and angiogenesis-regulating potential of mesenchymal stem cells." FEBS Lett **589**(6): 710-717.

Comegna, M., M. Succoio, M. Napolitano, M. Vitale, C. D'Ambrosio, A. Scaloni, F. Passaro, N. Zambrano, F. Cimino and R. Faraonio (2014). "Identification of miR-494 direct targets involved in senescence of human diploid fibroblasts." FASEB J **28**(8): 3720-3733.

Dahlman, J. E., K. J. Kauffman, R. Langer and D. G. Anderson (2014). "Nanotechnology for in vivo targeted siRNA delivery." Adv Genet **88**: 37-69.

DeLisser, H. M. (2009). "CD44: target for antiangiogenesis therapy." Blood **114**(25): 5114-5115.

Dimitrova, N. and T. de Lange (2009). "Cell cycle-dependent role of MRN at dysfunctional telomeres: ATM signaling-dependent induction of nonhomologous end joining (NHEJ) in G1 and resection-mediated inhibition of NHEJ in G2." Mol Cell Biol **29**(20): 5552-5563.

Dzikiewicz-Krawczyk, A. (2008). "The importance of making ends meet: mutations in genes and altered expression of proteins of the MRN complex and cancer." Mutat Res **659**(3): 262-273.

Ebert, M. S. and P. A. Sharp (2012). "Roles for microRNAs in conferring robustness to biological processes." Cell **149**(3): 515-524.

Economopoulou, M., H. F. Langer, A. Celeste, V. V. Orlova, E. Y. Choi, M. Ma, A. Vassilopoulos, E. Callen, C. Deng, C. H. Bassing, M. Boehm, A. Nussenzweig and T. Chavakis (2009). "Histone H2AX is integral to hypoxia-driven neovascularization." Nat Med **15**(5): 553-558.

Esser, J. S., E. Saretzki, F. Pankratz, B. Engert, S. Grundmann, C. Bode, M. Moser and Q. Zhou (2017). "Bone morphogenetic protein 4 regulates microRNAs miR-494 and miR-126-5p in control of endothelial cell function in angiogenesis." Thromb Haemost.

Fish, J. E. and D. Srivastava (2009). "MicroRNAs: opening a new vein in angiogenesis research." Sci Signal **2**(52): pe1.

Flynn, K. M., M. Michaud, S. Canosa and J. A. Madri (2013). "CD44 regulates vascular endothelial barrier integrity via a PECAM-1 dependent mechanism." Angiogenesis **16**(3): 689-705.

Gao, R., R. Singh, Z. Kaul, S. C. Kaul and R. Wadhwa (2015). "Targeting of DNA Damage Signaling Pathway Induced Senescence and Reduced Migration of Cancer cells." J Gerontol A Biol Sci Med Sci **70**(6): 701-713.

Garner, K. M., A. A. Pletnev and A. Eastman (2009). "Corrected structure of mirin, a small-molecule inhibitor of the Mre11-Rad50-Nbs1 complex." Nat Chem Biol **5**(3): 129-130; author reply 130.

Gates, P. E., W. D. Strain and A. C. Shore (2009). "Human endothelial function and microvascular ageing." Exp Physiol **94**(3): 311-316.

Inui, M., G. Martello and S. Piccolo (2010). "MicroRNA control of signal transduction." Nat Rev Mol Cell Biol **11**(4): 252-263.

Jin, Y., S. D. Tymen, D. Chen, Z. J. Fang, Y. Zhao, D. Dragas, Y. Dai, P. T. Marucha and X. Zhou (2013). "MicroRNA-99 family targets AKT/mTOR signaling pathway in dermal wound healing." PLoS One **8**(5): e64434.

Ju, Y. J., K. H. Lee, J. E. Park, Y. S. Yi, M. Y. Yun, Y. H. Ham, T. J. Kim, H. M. Choi, G. J. Han, J. H. Lee, J. Lee, J. S. Han, K. M. Lee and G. H. Park (2006). "Decreased expression of DNA repair proteins Ku70 and Mre11 is associated with aging and may contribute to the cellular senescence." Exp Mol Med **38**(6): 686-693.

Kane, N. M., L. Howard, B. Descamps, M. Meloni, J. McClure, R. Lu, A. McCahill, C. Breen, R. M. Mackenzie, C. Delles, J. C. Mountford, G. Milligan, C. Emanueli and A. H. Baker (2012). "Role of microRNAs 99b, 181a, and 181b in the differentiation of human embryonic stem cells to vascular endothelial cells." Stem Cells **30**(4): 643-654.

Kurz, D. J., S. Decary, Y. Hong, E. Trivier, A. Akhmedov and J. D. Erusalimsky (2004). "Chronic oxidative stress compromises telomere integrity and accelerates the onset of senescence in human endothelial cells." Journal of Cell Science **117**(11): 2417-2426.

Lafrance-Vanasse, J., G. J. Williams and J. A. Tainer (2015). "Envisioning the dynamics and flexibility of Mre11-Rad50-Nbs1 complex to decipher its roles in DNA replication and repair." Prog Biophys Mol Biol **117**(2-3): 182-193.

Landskroner-Eiger, S., I. Moneke and W. C. Sessa (2013). "miRNAs as modulators of angiogenesis." Cold Spring Harb Perspect Med **3**(2): a006643.

Li, X., J. J. Cassidy, C. A. Reinke, S. Fischboeck and R. W. Carthew (2009). "A MicroRNA Imparts Robustness against Environmental Fluctuation during Development." Cell **137**(2): 273-282.

Li, Y., Y. Shen, P. Hohensinner, J. Ju, Z. Wen, Stuart B. Goodman, H. Zhang, Jörg J. Goronzy and Cornelia M. Weyand (2016). "Deficient Activity of the Nuclease MRE11A Induces T Cell Aging and Promotes Arthritogenic Effector Functions in Patients with Rheumatoid Arthritis." Immunity **45**(4): 903-916.

Liu, Y., X. Li, S. Zhu, J. G. Zhang, M. Yang, Q. Qin, S. C. Deng, B. Wang, K. Tian, L. Liu, Y. Niu, C. Y. Wang and G. Zhao (2015). "Ectopic expression of miR-494 inhibited the proliferation, invasion and chemoresistance of pancreatic cancer by regulating SIRT1 and c-Myc." Gene Ther **22**(9): 729-738.

Lukamowicz-Rajska, M., C. Mittmann, M. Prummer, Q. Zhong, J. Bedke, J. Hennenlotter, A. Stenzl, A. Mischo, S. Bihr, M. Schmidinger, U. Vogl, I. Blume, C. Karlo, P. Schraml and H. Moch (2016). "MiR-99b-5p expression and response to tyrosine kinase inhibitor treatment in clear cell renal cell carcinoma patients." Oncotarget **7**(48): 78433-78447.

Minamino, T., H. Miyauchi, T. Yoshida, Y. Ishida, H. Yoshida and I. Komuro (2002). "Endothelial Cell Senescence in Human Atherosclerosis." Role of Telomere in Endothelial Dysfunction **105**(13): 1541-1544.

Mun, G. I. and Y. C. Boo (2010). "Identification of CD44 as a senescence-induced cell adhesion gene responsible for the enhanced monocyte recruitment to senescent endothelial cells." American Journal of Physiology - Heart and Circulatory Physiology **298**(6): H2102-H2111.

O'Malley, B. W., Jr., D. Li, J. Carney, J. Rhee and M. Suntharalingam (2003). "Molecular disruption of the MRN(95) complex induces radiation sensitivity in head and neck cancer." Laryngoscope **113**(9): 1588-1594.

Ohdaira, H., M. Sekiguchi, K. Miyata and K. Yoshida (2012). "MicroRNA-494 suppresses cell proliferation and induces senescence in A549 lung cancer cells." Cell Prolif **45**(1): 32-38.

Okuno, Y., A. Nakamura-Ishizu, K. Otsu, T. Suda and Y. Kubota (2012). "Pathological neoangiogenesis depends on oxidative stress regulation by ATM." Nat Med **18**(8): 1208-1216.

Orian-Rousseau, V., L. Chen, J. P. Sleeman, P. Herrlich and H. Ponta (2002). "CD44 is required for two consecutive steps in HGF/c-Met signaling." Genes & Development **16**(23): 3074-3086.

Osella, M., C. Bosia, D. Corá and M. Caselle (2011). "The Role of Incoherent MicroRNA-Mediated Feedforward Loops in Noise Buffering." PLoS Computational Biology **7**(3): e1001101.

Ponta, H., L. Sherman and P. A. Herrlich (2003). "CD44: From adhesion molecules to signalling regulators." Nat Rev Mol Cell Biol **4**(1): 33-45.

Porro, A., S. Feuerhahn and J. Lingner (2014). "TERRA-reinforced association of LSD1 with MRE11 promotes processing of uncapped telomeres." Cell Rep **6**(4): 765-776.

Rai, R., C. Hu, C. Broton, Y. Chen, M. Lei and S. Chang (2017). "NBS1 Phosphorylation Status Dictates Repair Choice of Dysfunctional Telomeres." Molecular Cell **65**(5): 801-817.e804.

Regina, C., E. Panatta, E. Candi, G. Melino, I. Amelio, C. R. Balistreri, M. Annicchiarico-Petruzzelli, N. Di Daniele and G. Ruvolo (2016). "Vascular ageing and endothelial cell senescence: Molecular mechanisms of physiology and diseases." Mech Ageing Dev **159**: 14-21.

Santulli, G. (2016). "MicroRNAs and Endothelial (Dys) Function." J Cell Physiol **231**(8): 1638-1644.

Schweighofer, B., J. Testori, C. Sturtzel, S. Sattler, H. Mayer, O. Wagner, M. Bilban and E. Hofer (2009). "The VEGF-induced transcriptional response comprises gene clusters at the crossroad of angiogenesis and inflammation." Thromb Haemost **102**(3): 544-554.

Shi, H., P. Li, W. Liang, J. Chen and Y. Gao (2010). "Mechanisms of microRNA-mediated regulation of angiogenesis." Front Biosci (Elite Ed) **2**: 1304-1319.

Tremmel, M., A. Matzke, I. Albrecht, A. M. Laib, V. Olaku, K. Ballmer-Hofer, G. Christofori, M. Héroult, H. G. Augustin, H. Ponta and V. Orian-Rousseau (2009). "A CD44v6 peptide reveals a role of CD44 in VEGFR-2 signaling and angiogenesis." Blood **114**(25): 5236-5244.

Uziel, T., Y. Lerenthal, L. Moyal, Y. Andegeko, L. Mittelman and Y. Shiloh (2003). "Requirement of the MRN complex for ATM activation by DNA damage." EMBO J **22**(20): 5612-5621.

Wang, X., X. Zhang, X. P. Ren, J. Chen, H. Liu, J. Yang, M. Medvedovic, Z. Hu and G. C. Fan (2010). "MicroRNA-494 targeting both proapoptotic and antiapoptotic proteins protects against ischemia/reperfusion-induced cardiac injury." Circulation **122**(13): 1308-1318.

Welten, S. M., A. J. Bastiaansen, R. C. de Jong, M. R. de Vries, E. A. Peters, M. C. Boonstra, S. P. Sheikh, N. La Monica, E. R. Kandimalla, P. H. Quax and A. Y. Nossent (2014). "Inhibition of 14q32 MicroRNAs miR-329, miR-487b, miR-494, and miR-495 increases neovascularization and blood flow recovery after ischemia." Circ Res **115**(8): 696-708.

Weng, J. H., C. C. Yu, Y. C. Lee, C. W. Lin, W. W. Chang and Y. L. Kuo (2016). "miR-494-3p Induces Cellular Senescence and Enhances Radiosensitivity in Human Oral Squamous Carcinoma Cells." Int J Mol Sci **17**(7).

Wezel, A., S. M. Welten, W. Razawy, H. M. Lagraauw, M. R. de Vries, E. A. Goossens, M. C. Boonstra, J. F. Hamming, E. R. Kandimalla, J. Kuiper, P. H. Quax, A. Y. Nossent and I. Bot (2015). "Inhibition of MicroRNA-494 Reduces Carotid Artery Atherosclerotic Lesion Development and Increases Plaque Stability." Ann Surg **262**(5): 841-848.

Williams, R. S. and J. A. Tainer (2007). "Learning our ABCs: Rad50 directs MRN repair functions via adenylate kinase activity from the conserved ATP binding cassette." Mol Cell **25**(6): 789-791.

Williams, R. S., J. S. Williams and J. A. Tainer (2007). "Mre11-Rad50-Nbs1 is a keystone complex connecting DNA repair machinery, double-strand break signaling, and the chromatin template." Biochem Cell Biol **85**(4): 509-520.

Wilson, R., C. Espinosa-Diez, N. Kanner, N. Chatterjee, R. Ruhl, C. Hipfinger, S. J. Advani, J. Li, O. F. Khan, A. Franovic, S. M. Weis, S. Kumar, L. M. Coussens, D. G. Anderson, C. C. Chen, D. A. Cheresh and S. Anand (2016). "MicroRNA regulation of endothelial TREX1 reprograms the tumour microenvironment." Nat Commun **7**: 13597.

Wu, Y., S. Xiao and X.-D. Zhu (2007). "MRE11-RAD50-NBS1 and ATM function as co-mediators of TRF1 in telomere length control." Nat Struct Mol Biol **14**(9): 832-840.

Zhao, J. J., J. Yang, J. Lin, N. Yao, Y. Zhu, J. Zheng, J. Xu, J. Q. Cheng, J. Y. Lin and X. Ma (2009). "Identification of miRNAs associated with tumorigenesis of retinoblastoma by miRNA microarray analysis." Childs Nerv Syst **25**(1): 13-20.

Zhuang, Y., H. Peng, V. Mastej and W. Chen (2016). "MicroRNA Regulation of Endothelial Junction Proteins and Clinical Consequence." Mediators Inflamm **2016**: 5078627.

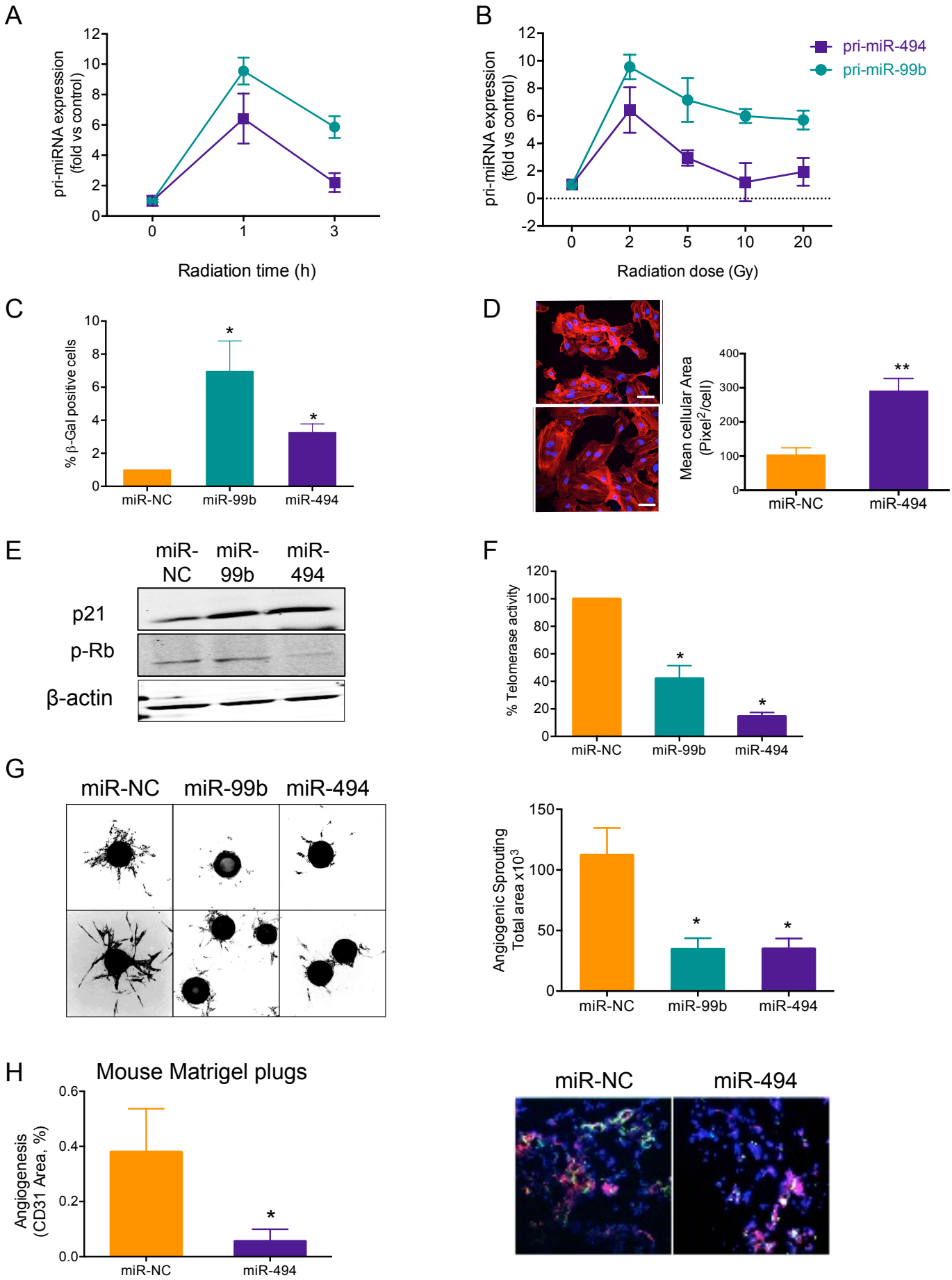
A
pri-miRNA expression (fold vs control)
Radiation time (h)
B
pri-miR-494
pri-miR-99b
pri-miRNA expression (fold vs control)
Radiation dose (Gy)
C
% β-Gal positive cells
miR-NC
miR-99b
miR-494
D
Mean cellular Area (Pixel²/cell)
miR-NC
miR-494
E
miR-NC
miR-99b
miR-494
p21
p-Rb
β-actin
F
% Telomerase activity
miR-NC
miR-99b
miR-494
G
miR-NC
miR-99b
miR-494
Angiogenic Sprouting Total area x10³
miR-NC
miR-99b
miR-494
H
Mouse Matrigel plugs
Angiogenesis (CD31 Area, %)
miR-NC
miR-494
miR-NC
miR-494

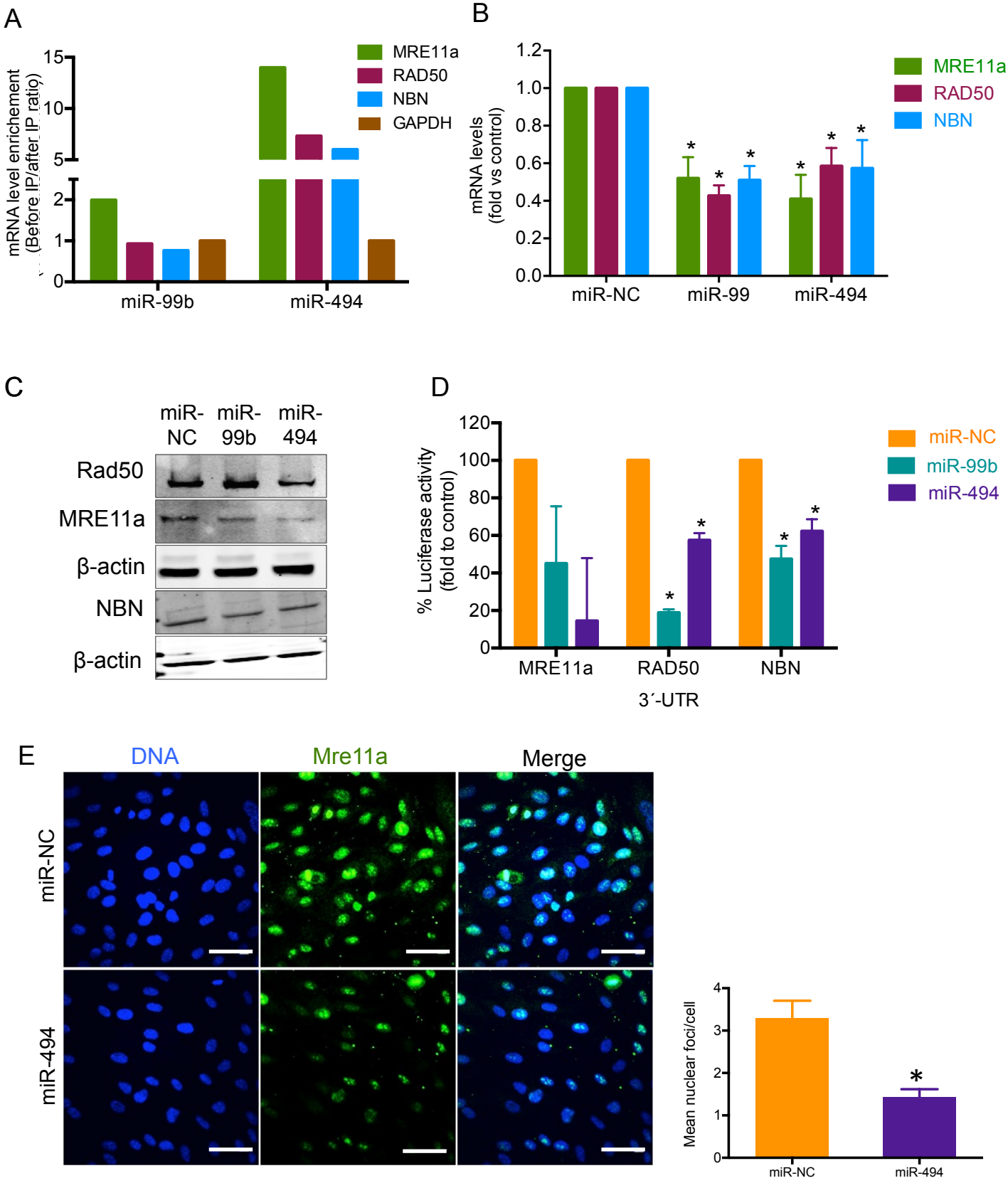
A
mRNA level enrichement (Before IP/after IP ratio)
15
10
5
2
1
0
MRE11a
RAD50
NBN
GAPDH
miR-99b
miR-494
B
mRNA levels (fold vs control)
1.2
1.0
0.8
0.6
0.4
0.2
0.0
MRE11a
RAD50
NBN
miR-NC
miR-99
miR-494
C
miR-NC
miR-99b
miR-494
Rad50
MRE11a
β-actin
NBN
β-actin
D
% Luciferase activity (fold to control)
120
100
80
60
40
20
0
miR-NC
miR-99b
miR-494
MRE11a
RAD50
NBN
3´-UTR
E
DNA
Mre11a
Merge
miR-NC
miR-494
Mean nuclear foci/cell
4
3
2
1
0
miR-NC
miR-494

A

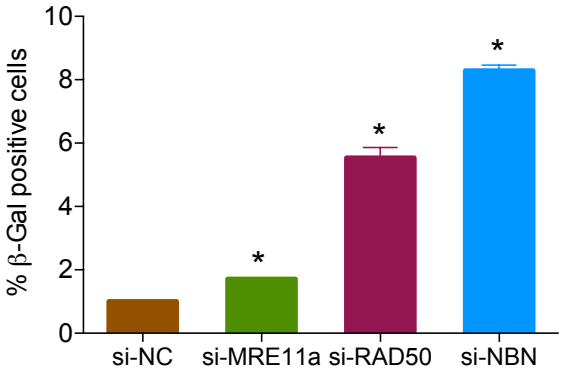
% β-Gal positive cells
10
8
6
4
2
0
*
*
*
si-NC
si-MRE11a
si-RAD50
si-NBN

B

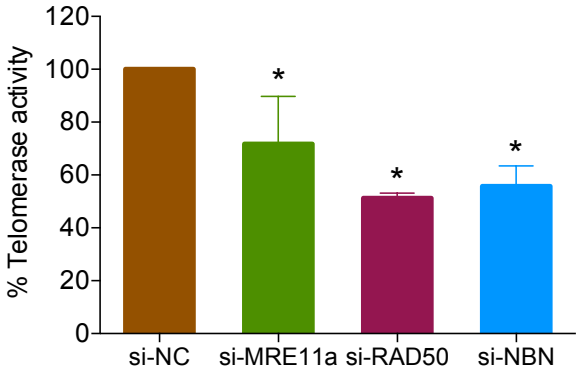
% Telomerase activity
120
100
80
60
40
20
0
*
*
*
si-NC
si-MRE11a
si-RAD50
si-NBN

C

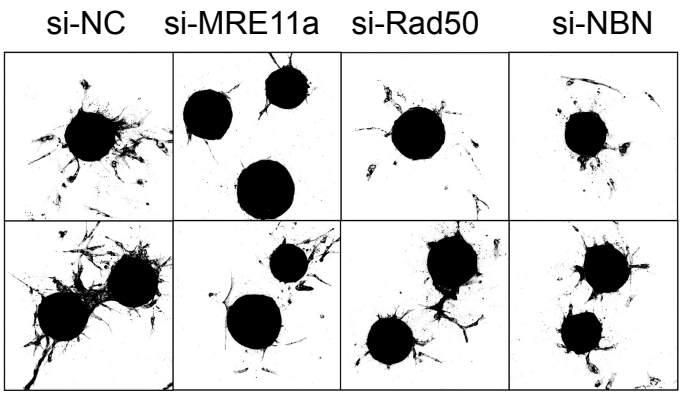
si-NC
si-MRE11a
si-Rad50
si-NBN

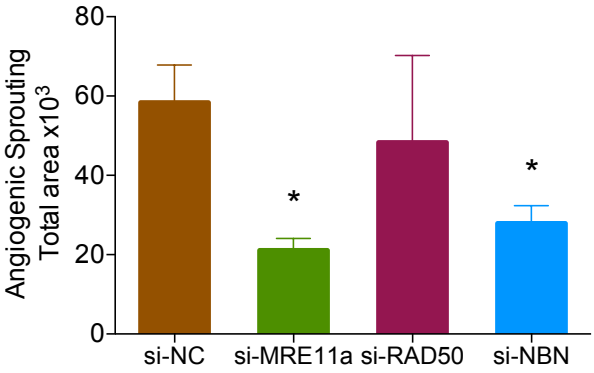
Angiogenic Sprouting
Total area x10³
80
60
40
20
0
*
*
si-NC
si-MRE11a
si-RAD50
si-NBN

D

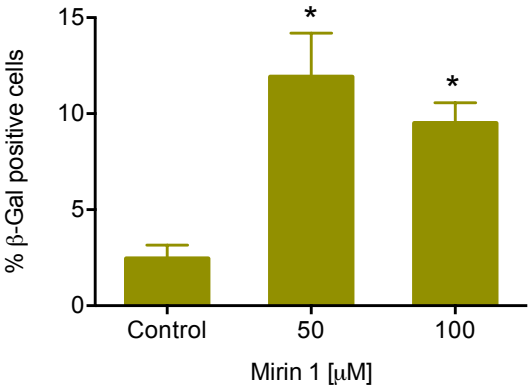
% β-Gal positive cells
15
10
5
0
*
*
Control
50
100
Mirin 1 [μM]

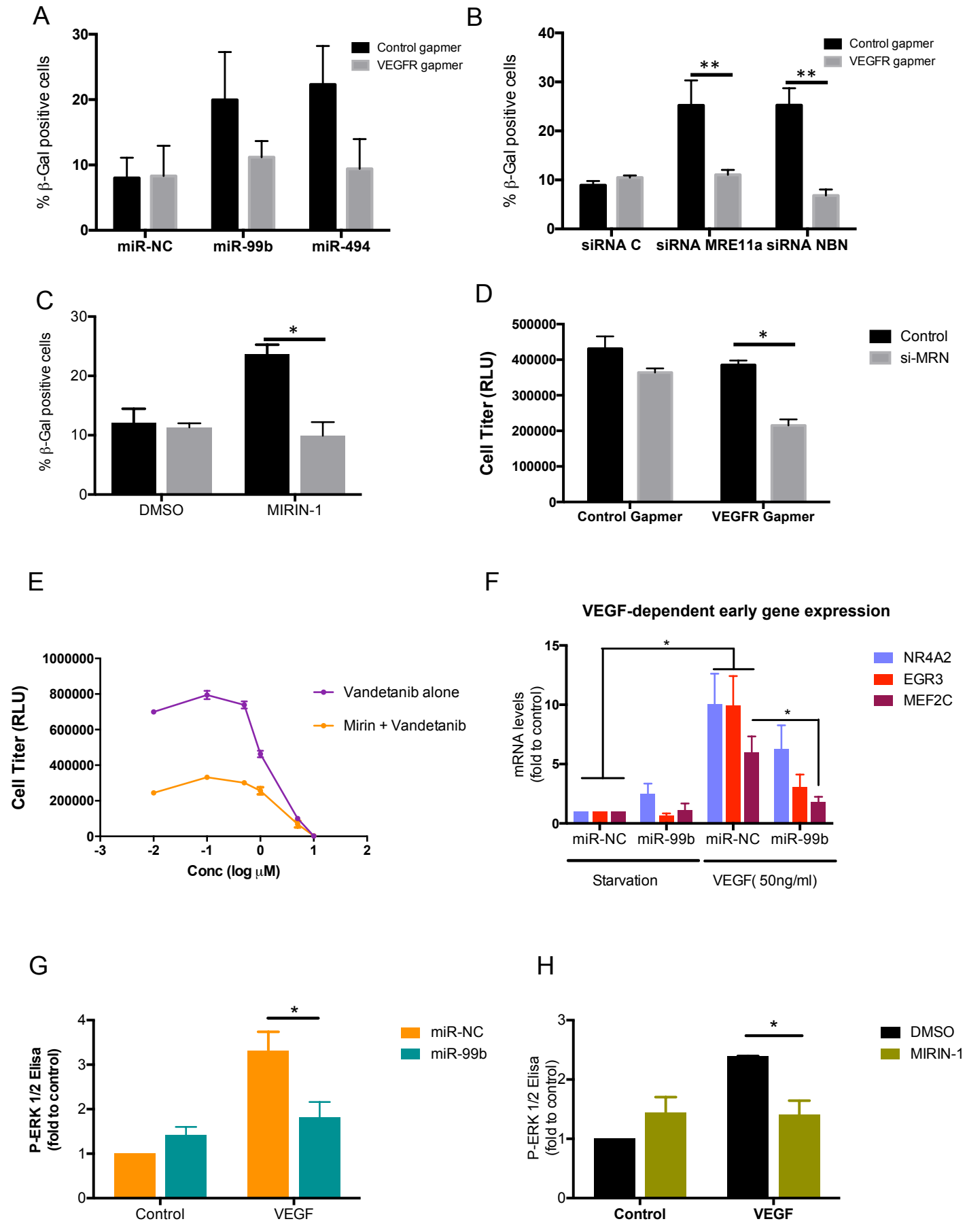
A
% β-Gal positive cells
Control gapmer
VEGFR gapmer
miR-NC
miR-99b
miR-494
B
% β-Gal positive cells
Control gapmer
VEGFR gapmer
**
**
siRNA C
siRNA MRE11a
siRNA NBN
C
% β-Gal positive cells
*
DMSO
MIRIN-1
D
Cell Titer (RLU)
*
Control
si-MRN
Control Gapmer
VEGFR Gapmer
E
Cell Titer (RLU)
Vandetanib alone
Mirin + Vandetanib
Conc (log μM)
F
VEGF-dependent early gene expression
mRNA levels (fold to control)
*
*
NR4A2
EGR3
MEF2C
miR-NC
miR-99b
miR-NC
miR-99b
Starvation
VEGF( 50ng/ml)
G
P-ERK 1/2 Elisa (fold to control)
*
miR-NC
miR-99b
Control
VEGF
H
P-ERK 1/2 Elisa (fold to control)
*
DMSO
MIRIN-1
Control
VEGF

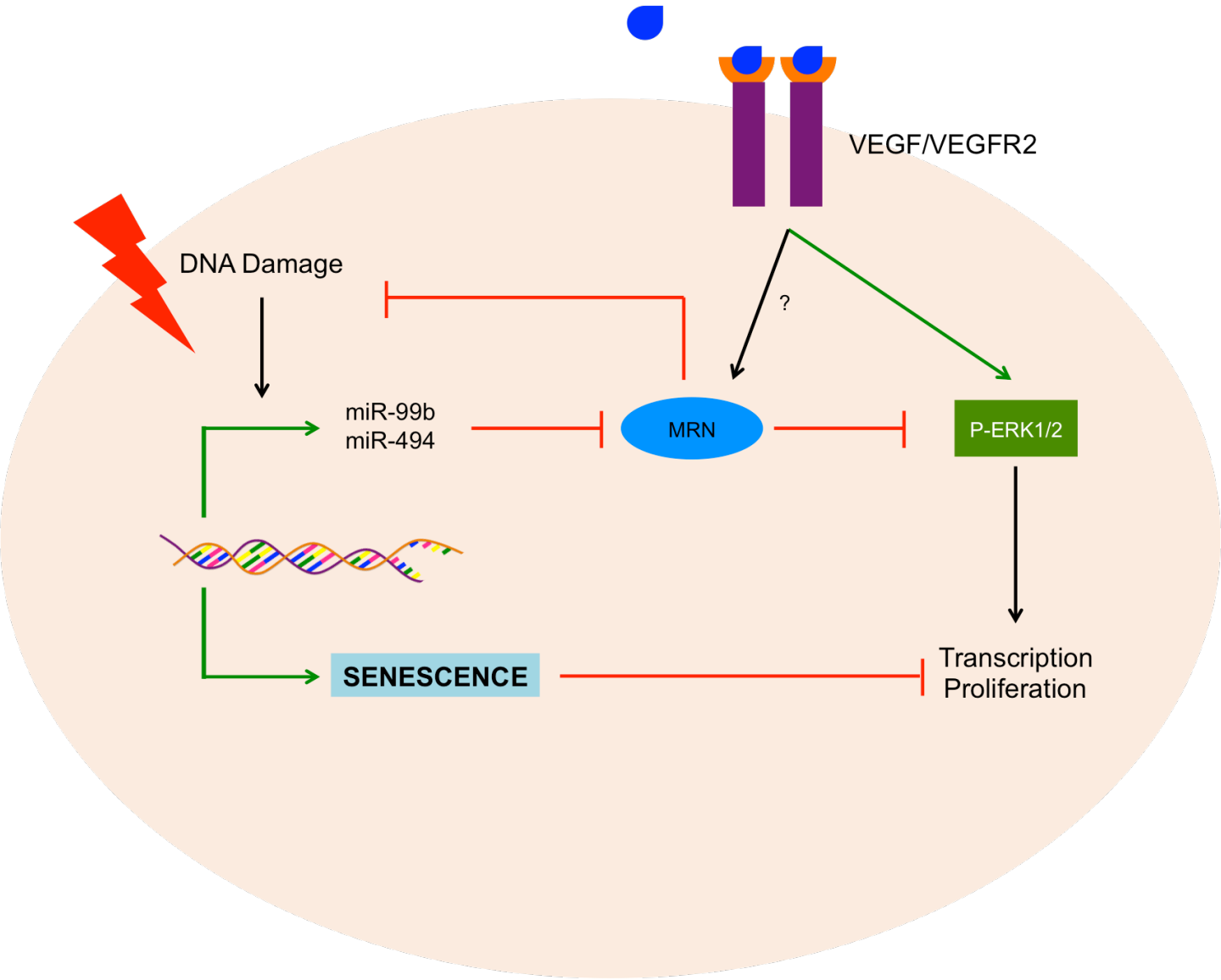
VEGF/VEGFR2
DNA Damage
?
miR-99b
miR-494
MRN
P-ERK1/2
SENESCENCE
Transcription
Proliferation

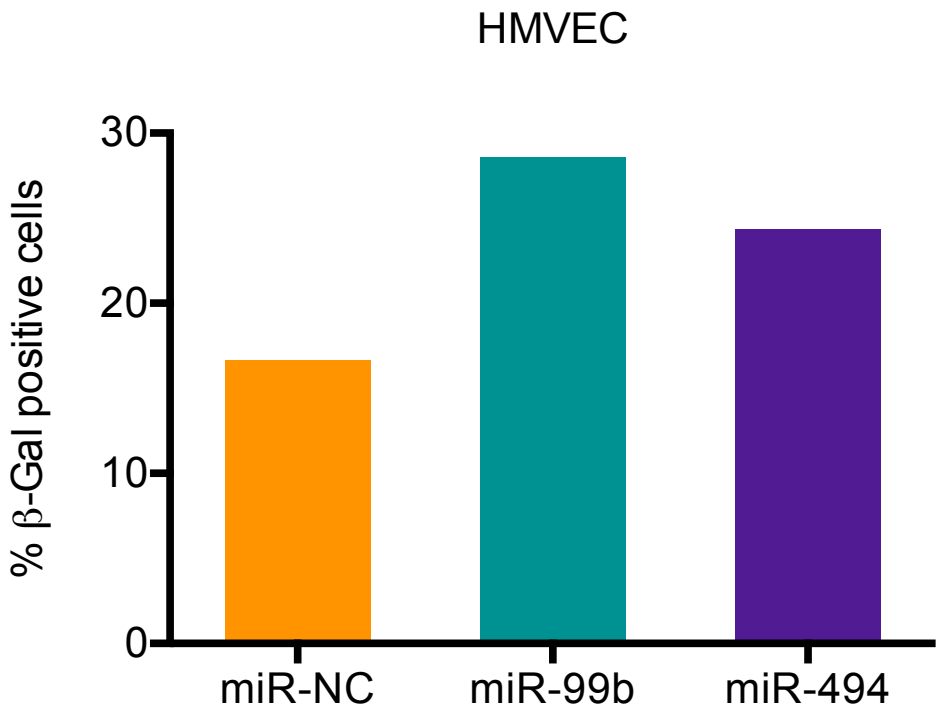
HMVEC
% β-Gal positive cells
30
20
10
0
miR-NC
miR-99b
miR-494

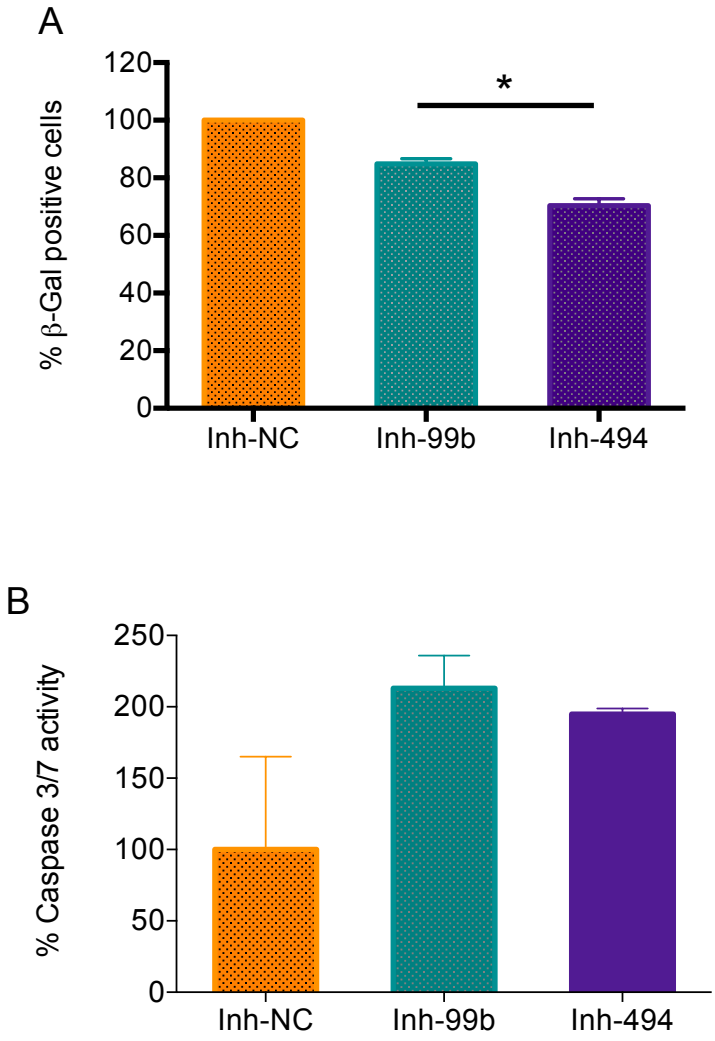
A
% β-Gal positive cells
120
100
80
60
40
20
0
*
Inh-NC
Inh-99b
Inh-494
B
% Caspase 3/7 activity
250
200
150
100
50
0
Inh-NC
Inh-99b
Inh-494

| Gene | miR-99b | miR-494 |
|---|---|---|
| APEX1 | 0.64 | 1.00 |
| ATM | 0.77 | 0.87 |
| ATR | 0.72 | 0.50 |
| BARD1 | 0.66 | 0.30 |
| BRCA1 | 0.23 | 0.52 |
| BRCA2 | 0.52 | 0.54 |
| CCNO | | 1.01 |
| CHECK1 | 0.37 | 0.52 |
| CHECK2 | 2.58 | 0.75 |
| DCLRE1A | 1.11 | 0.90 |
| ERCC1 | 1.36 | 0.86 |
| ERCC2 | 2.74 | 1.06 |
| ERCC3 | 0.57 | 0.74 |
| ERCC4 | 0.42 | 0.72 |
| ERCC5 | 0.97 | 0.66 |
| ERCC6 | 0.19 | 0.51 |
| ERCC8 | 1.03 | 0.97 |
| FANCA | 0.99 | 0.83 |
| FANCC | 2.34 | 0.58 |
| FANCD2 | 0.23 | 0.63 |
| FANCE | 2.38 | 1.04 |
| FANCF | 1.19 | 0.63 |
| FANCG | 1.69 | 0.76 |
| FEN1 | 1.67 | 0.69 |
| GADD45A | 0.75 | 0.75 |
| GADD45B | 2.13 | 1.18 |
| GADD45G | 1.12 | 0.53 |
| GTF2H1 | 0.26 | 0.55 |
| GTF2H3 | 0.47 | 0.70 |
| HUS1 | 0.80 | 0.66 |
| IGF1 | | |
| LIG1 | 3.74 | 0.96 |
| LIG3 | 0.54 | 0.80 |
| LIG4 | 0.61 | 0.77 |
| MAPK10 | | |
| MAPK11 | 8.37 | 1.39 |
| MAPK12 | 2.51 | 0.98 |
| MAPK14 | 0.33 | 0.78 |
| MAPK8 | 0.36 | 0.60 |
| MAPK9 | 0.32 | 0.64 |
| MBD4 | 0.48 | 0.61 |
| MDM2 | 0.49 | 1.24 |
| MGMT | 3.48 | 0.88 |
| MRE11A | 0.25 | 0.44 |
| MSH2 | 0.30 | 0.69 |
| MSH3 | 0.63 | 0.53 |

| Gene | miR-99b | miR-494 |
|---|---|---|
| MSH6 | 0.52 | 0.80 |
| NBN | 0.24 | 0.36 |
| NTHL1 | 4.00 | 1.07 |
| OGG1 | 2.50 | 1.38 |
| PARP1 | 0.37 | 0.70 |
| PCNA | 0.54 | 0.82 |
| PNKP | 3.23 | 1.43 |
| POLA1 | 1.03 | 0.77 |
| POLB | 0.93 | 0.67 |
| POLD1 | 13.99 | 0.62 |
| POLG | 2.08 | 0.95 |
| POLH | 0.60 | 0.87 |
| POLK | 0.47 | 0.41 |
| POLQ | 0.44 | 0.30 |
| POLR1B | 0.35 | 0.90 |
| POLR1C | 1.19 | 0.92 |
| POLR2A | 1.32 | 0.69 |
| POLR2B | 0.15 | 0.57 |
| POLR2C | 0.85 | 1.15 |
| PRKDC | 0.19 | 0.66 |
| PSMA3 | 0.99 | 0.50 |
| PSMB10 | 4.91 | 0.80 |
| PSMB5 | 2.19 | 0.73 |
| PSMB8 | 5.85 | 0.84 |
| PSMB9 | 0.57 | 0.47 |
| PSMC4 | 0.68 | 0.73 |
| RAD1 | 0.77 | 0.72 |
| RAD17 | 0.73 | 0.77 |
| RAD23B | 0.24 | 0.66 |
| RAD50 | 0.31 | 0.49 |
| RAD51 | 0.70 | 0.58 |
| RAD52 | 0.70 | 0.60 |
| RAD9A | 1.15 | 0.91 |
| RPA2 | 0.92 | 0.69 |
| RPA3 | | |
| SMUG1 | 5.70 | 1.12 |
| TP53 | 0.76 | 0.92 |
| TREX1 | 0.70 | 0.54 |
| TREX2 | | 1.12 |
| XAB2 | 1.37 | 0.99 |
| XPA | 1.02 | 1.05 |
| XPC | 0.64 | 1.05 |
| XRCC1 | 0.69 | 0.67 |
| XRCC4 | 0.44 | 0.73 |
| XRCC5 | 0.26 | 0.63 |
| XRCC6 | 1.03 | 0.66 |

Numbers indicate fold change vs GAPDH

A

```
4021 GCACGGTGGCTCACGCCTGTGATCCTAGCACTTTGGGAGGCCAAAGCAGGCGGATCACCT
4081 GAGGTCAGGAGTTCGAGACCAGCAGGGCCAACATGGCGAAACCCCGACTCTACTAAAAAT
4141 ACAAAAATTAGCCAGGCATGGTGGTGGGCGCCTGTAATCCCAACTACTCAGGAGGCTGAG
4201 GCAGGAGAATTGCTTGAACCTGGGAGTTGGAGGTCACGGTGAGCTGATATCACGCCATTG
4261 CACTCCAGCCTGGGCAACAGAGCAAGACTCTGTCTCAATCAATCTATCCATCAATCGATA
4321 AGAACCCCAGATTGTATAGCTACATGTTTTAGCCCCCTTTTCAAAGTATATGTTCTCCTT
4381 GGTACTTATTTTGACATTCTGACTTTTCTACATATGCTTTATCAACCTCTTAATTAAACC
4441 ATCATTGTCTATTTTGAGAGATAACTGCGCTGCTTCCCGTTGTGTGTTTTAAATGTTATT
4501 GTTCAGTTTGAGTCAAATAAAAGGATATTTAATCTGTGGTGCCTTGA
```

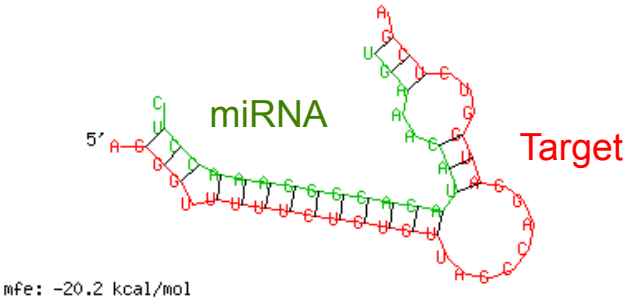


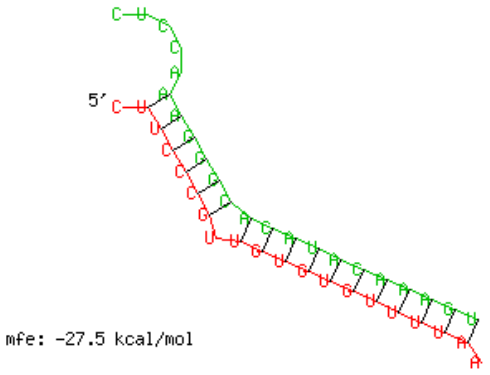


B

```
1801 TTGCAAGTTAAAACAGACTTCCCAATTTTAAATCTGGTTTCCCCCTGAATATGTGGCATC
1861 CTTGGCAGCACTTCTGAGAGTGGCTGCTTTCATTCCAAGAAGCCCATGGGTTTGGAGGTG
1921 GGATAGGTGCCTTTCTGGCTTCTCATTGCTGCTTCTAGATCAGTCTCCAAATATCCCCCT
```

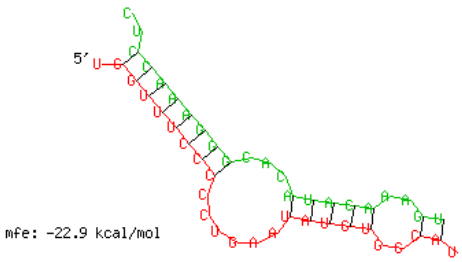


C

```
1621 TTTTCCTTTTTAACCATTCCAATCGGTGTGTAGTGATGTTTCATTTTGGTTTTAATTTGT
1681 ATATCCCTGATAGCTATAATTGGGTCATAGAAATTCTTTATACATTCTAGATGCAAGTCT
1741 CTTGTCGGATATATGTATTGAGATATTACACCTAGTCTGTGGCTTGACTGTTTTCTTTAT
```

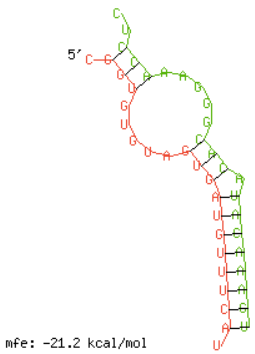

A

```
1561 ACCTACCCCTGCACAAGCCATGCTGGCTCAGTCTGAGCTGTGGGCCACATCAGCTAGTGG
1621 CTCTTCTCATGCATCAGTTAGGTGGGTCTGGGTGAGAGTTATAGTGAGGGAATGGTCACT
1681 AAAGTATCCTGACAAGTTCCTAGGAAAAAAGGAATAAAGTTTTTTTCCTTAAAAAAAAAA
1741 AAATTGCTCTTGGCTGTGAAAAGAGGTACTAAATGCGATTCAGTTCACCGCTAAGGAAAG
1861 AATACTATGTATCAAGCCCTGAAAATATGGTAAATAAAACGTGACAGGGAAACCTTTTTT
1921 TGATTGAATATTGTTACATAGTTAAATGTGCTATATATCCTTAATATTTTATATTGATCC
1981 TGCAAAATCTGTTGGTTTTAGGGGAGTTTTGTTTTTTGTTTCTAACAATTTTCAGACCTG
2041 TTGGTATAGGAATGTAGAAGTCTTTCAGATGATTTGAAAGCAGCTGCATTTGCTCTTGGA
```

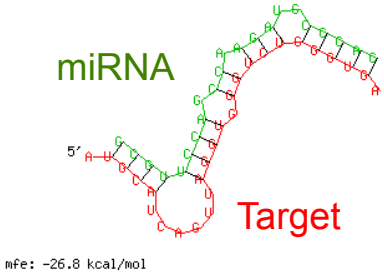


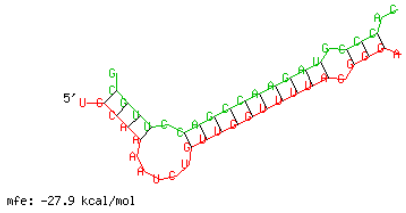


B

```
1261 CTAGAACCCGTGACTGTTACTTTATACAGCAAAGGAAACTTTGCAGATGTGATTAAAGCT
1321 AAGGACCTTAAGACAGAGTATCCTGGGGGTGGTGGTGGGGTGGGGGGGGGGTCCTAAATGT
1381 AATCACGAGTAAGATTAAGAGCAAATCAATTCTAGTCATATATTAAACATCCACAATAAC

3601 GTAGTCTCAGCTACTTGGCTGAGATAGGATCCCTGGAGTCTGAGGGTTCAAGGCTGCAGT
3661 GAGCTGTGATTTGTGCCACTGCACCCCAGCCTGGGTGGGTGGCAGAGTGAGACCCTGTCT
3721 AAAAAGACAAAAAAAAAAAAAAAAAAAAAGCAGCAGCAGCTGAAAGTTGGCAGGAGCACA
```

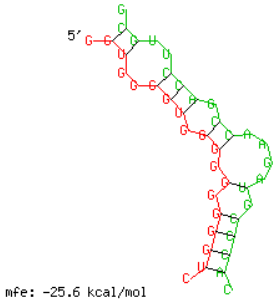



C

```
661 TTTTCACCAGAATGGAAAGACCTGTACCCCTTTTTGGTGGTCTTACTGAGCTGGGTGGGT
721 GTCTGTTTTGAGCTTATTTAGAGTCCTAGTTTTCCTACTTATAAAGTAGAAATGGTGAGA
781 TTGTTTTCTTTTTCTACCTTAAAGGGAGATGGTAAGAAACAATGAATGTCTTTTTTCAAA

1141 CAGCTGCAAGGGAGTTAGGGAAATGAAGGTCTTTTTTTAAAAGCTTCTCAGCCTTCCTAG
1201 GGAACAGAAATTGGGTGAGCCAATCTGCAATTTCTACTACAGGCATTGAGACCAGTTAGA
1261 TTATTGAAATATTATAGAGAGTTATGAACACTTAAATTATGATAGTGGTATGACATTGGA
```

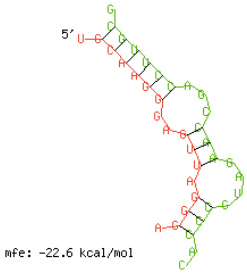


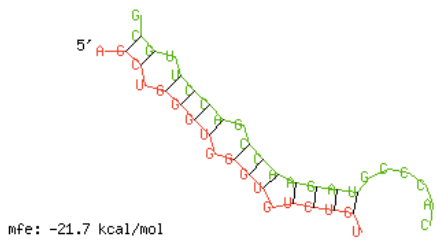

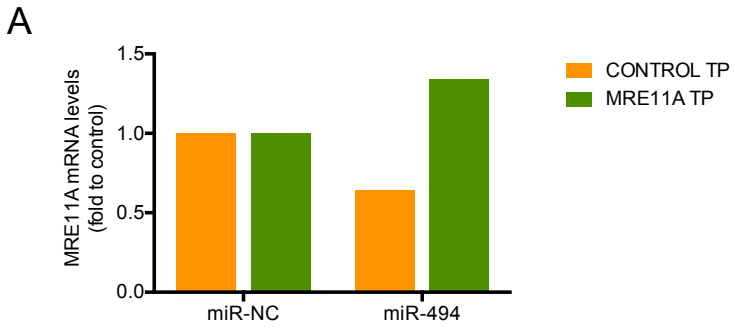
A
MRE11A mRNA levels
(fold to control)
1.5
1.0
0.5
0.0
miR-NC
miR-494
CONTROL TP
MRE11A TP

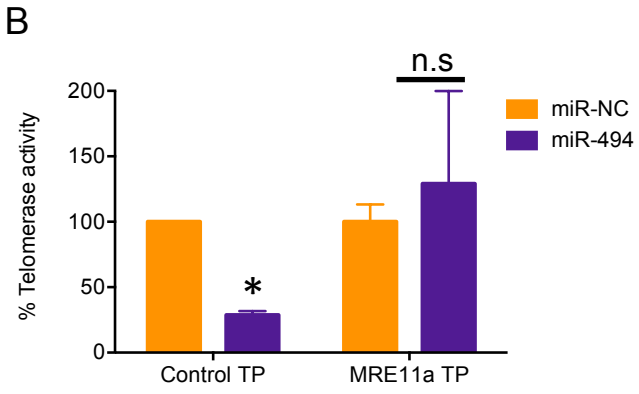
B
% Telomerase activity
200
150
100
50
0
n.s
*
Control TP
MRE11a TP
miR-NC
miR-494

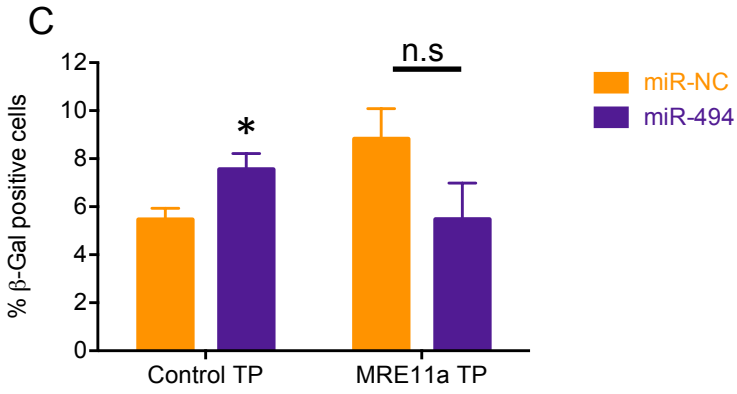
C
% β-Gal positive cells
12
10
8
6
4
2
0
n.s
*
Control TP
MRE11a TP
miR-NC
miR-494

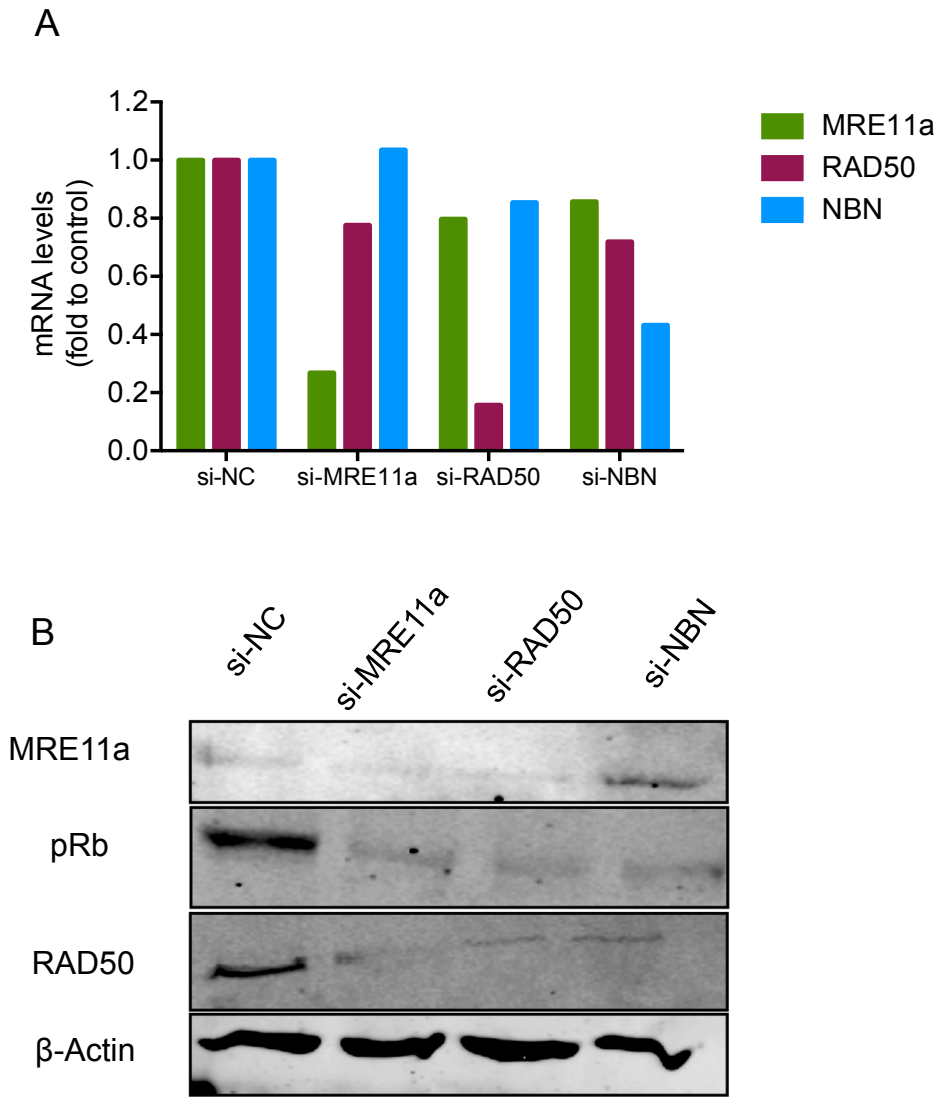
A
mRNA levels (fold to control)
1.2
1.0
0.8
0.6
0.4
0.2
0.0
si-NC
si-MRE11a
si-RAD50
si-NBN
MRE11a
RAD50
NBN
B
si-NC
si-MRE11a
si-RAD50
si-NBN
MRE11a
pRb
RAD50
β-Actin

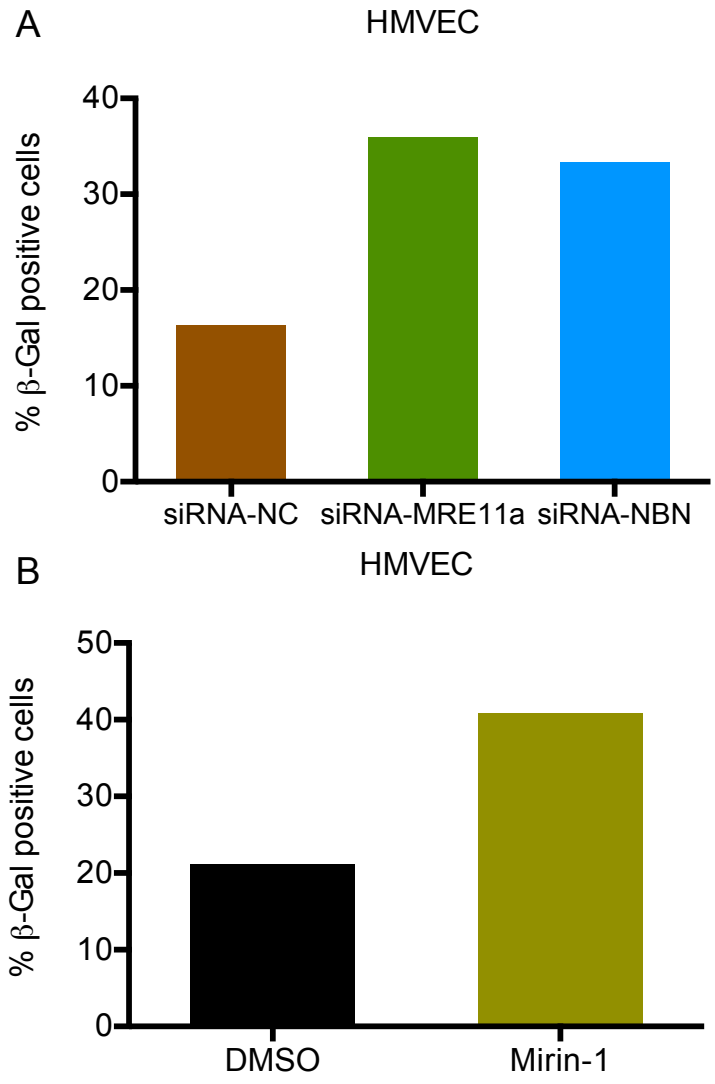
A
HMVEC
% β-Gal positive cells
40
30
20
10
0
siRNA-NC
siRNA-MRE11a
siRNA-NBN
B
HMVEC
% β-Gal positive cells
50
40
30
20
10
0
DMSO
Mirin-1

A

## Senescence gene array

| | miR-99b | miR-494 | si-MRN | si-NBN |
|---|---|---|---|---|
| CD44 | 23.61 | 40.84 | 2.19 | 2.3 |
| CDKN2D | 0.71 | 0.92 | 0.76 | 1.11 |
| CHECK2 | 0.62 | 0.84 | 0.66 | 0.32 |
| COL1A1 | 0.43 | 1.5 | 0.41 | 0.75 |
| CREG1 | 0.69 | 0.95 | 0.64 | 0.61 |
| SOD2 | 0.49 | 0.79 | 0.25 | 0.26 |
| GAPDH | 1 | 1 | 1 | 1 |

B

## CD44 expression